NUCLEAR INSTRUMENTS AND METHODS 126 (1975) 477-491; © NORTH-HOLLAND PUBLISHING CO.

A STREAMER-CHAMBER DETECTOR AT THE CERN INTERSECTING STORAGE RINGS

K. EGGERT and W. THOMÉ

III. Physikalisches Institut der Technischen Hochschule, Aachen, Germany

B. BETEV*, G. BOHM**, P. DARRIULAT, P. DITTMANN, E. GYGI, M. HOLDER, K. T. McDONALD, H. G. PUGH† and F. SCNHEIDER

CERN, Geneva, Switzerland

H. ALBRECHT, T. MODIS and K. TITTEL

Institut für Hochenergiephysik, Heidelberg, Germany

I. DERADO, V. ECKARDT, H. J. GEBAUER, R. MEINKE, O. R. SANDER†† and P. SEYBOTH

Max-Planck-Institut für Physik und Astrophysik, Munich, Germany

Received 20 March 1975

The design, construction, and performance of a streamer-chamber system for the study of inelastic proton–proton collisions at the CERN ISR are described. The chambers have specially shaped ground electrodes to accommodate the ISR vacuum chamber and to obtain an almost 4π solid angle. Problems arising from the non-flat electrodes and the insertion of converter plates into the sensitive volume of the chambers are discussed. The high-voltage and gas system are described and in particular the control system for the streamer-chamber memory time which is essential for operation at high ISR luminosities. The optical system, including single-stage electrostatic image intensifiers, is explained. The chambers are triggered on inelastic beam–beam interactions with counter hodoscopes, or on interactions including a photon which is detected in a lead-glass Cherenkov counter located at 90°. Finally the analysis of the pictures is described.

1. Introduction

For an investigation of the nature of proton–proton collisions at the CERN ISR, we have chosen two topics: the general structure of the final state of inelastic proton–proton collisions, and the structure of those rarer collisions in which a particle emerges with large transverse momentum.

In this paper we describe the apparatus used to study these two phenomena concurrently.

A complete observation of the outcome of a high-energy collision would consist of the four-momenta and quantum numbers of all particles produced. However, it is known, both from studies with cosmic rays and particle accelerators, that while a large number (typically 18 at ISR energies) of particles are produced, they are predominantly pions, whose transverse momenta are small, averaging 300 MeV/c. Hence the first general investigation of the entire final state may reasonably restrict itself to the measurement of angular variables. This restriction allows a technically simple "first-generation" experiment in which no magnetic field is needed. Some such limitation is certainly in order, as there is no general method for the analysis and presentation of all possible effects in reactions producing typically 18 particles. We have attempted to study all of the particles, but with only a limited description of each.

Conceptually, the most simple use of the data to be obtained involves only counting the particles to yield topological cross sections (i.e. multiplicity distributions). The analysis which makes the most general use of the angular variables, and which may be applied over a restricted angular range if necessary, consists of determining the angular correlation among particles.

In the case of the high-transverse-momentum phenomena, we observe such general features as the change in total multiplicity with transverse momentum of one particle, and infer the topology of the excess of particles which provides the momentum balance.

With the preceding motivation, we desired a large solid angle detector, which should be triggerable to select specific events, and should detect neutral particles (primarily photons) as well as charged

* On leave from Institute of Nuclear Research, Sofia, Bulgaria.
** On leave from Institute of Nuclear Research, Dubna, USSR.
† On leave from University of Maryland, College Park, Md., U.S.A.
†† Now at University of California, Los Angeles, U.S.A.

particles. Anticipating the need to recognize complex topologies and reject sizeable backgrounds of particles from sources other than the primary interaction, we preferred an optical detector. These requirements indicated the use of a streamer chamber – a triggerable, large-volume optical device with nearly isotropic detection efficiency.

The configuration of such a detector is largely influenced by the geometry of the beam pipes and the vacuum chamber which contain the ISR beams. In the design presented below, the central vacuum chamber is surrounded by two streamer chambers, one above and one below the beam pipes. To retain a maximum solid angle, the innermost ground electrodes of the chambers are tailored to the shape of the vacuum chamber. With this solution, the full solid angle is covered, except for an equatorial gap of 8 cm between the two chambers.

The chambers should be large enough to observe tracks at forward production angles, and yet small enough that an entire chamber can be photographed with one camera. In practice, particles produced at small angles to the beams pass through the 3 mm stainless-steel wall of the beam pipes and are likely to interact. To minimize this effect, a thin-walled "bicone" vacuum chamber[1]) of length 128 cm was used, such that particles at angles of more than 40 mrad traverse very little material. From these considerations, the chamber length was chosen as 270 cm, with a width of 125 cm and a height of 50 cm.

To obtain information on a sizeable fraction of all photons produced, lead-oxide converter plates are installed inside the active volumes of the chambers. The arrangement of the 1 radiation-length-thick plates is such that they extend over all values of the rapidity variable, and convert about 35 % of all γ rays produced. Furthermore, some information about particles with small momenta can be obtained due to the stopping power of the converter plates.

In order to utilize the high luminosity of the ISR, it is necessary to reduce the streamer-chamber memory time to a minimum. As discussed below, stable memory times of between 1 and 2 μs were achieved, which allowed the experiment to operate at luminosities up to 5×10^{30} cm^{-2} s^{-1}, corresponding to an interaction rate of 200 kHz.

In addition, for the study of large-transverse-momentum phenomena, we have used an array of 61 hexagonal lead-glass blocks at 90° to the beams, which provide a trigger on π^0 via their two-photon decay.

The pulse heights in the glass blocks, various trigger parameters, and chamber and beam monitors are recorded on magnetic tape after processing by an on-line Hewlett-Packard 2100 computer.

In the following sections we present details of the

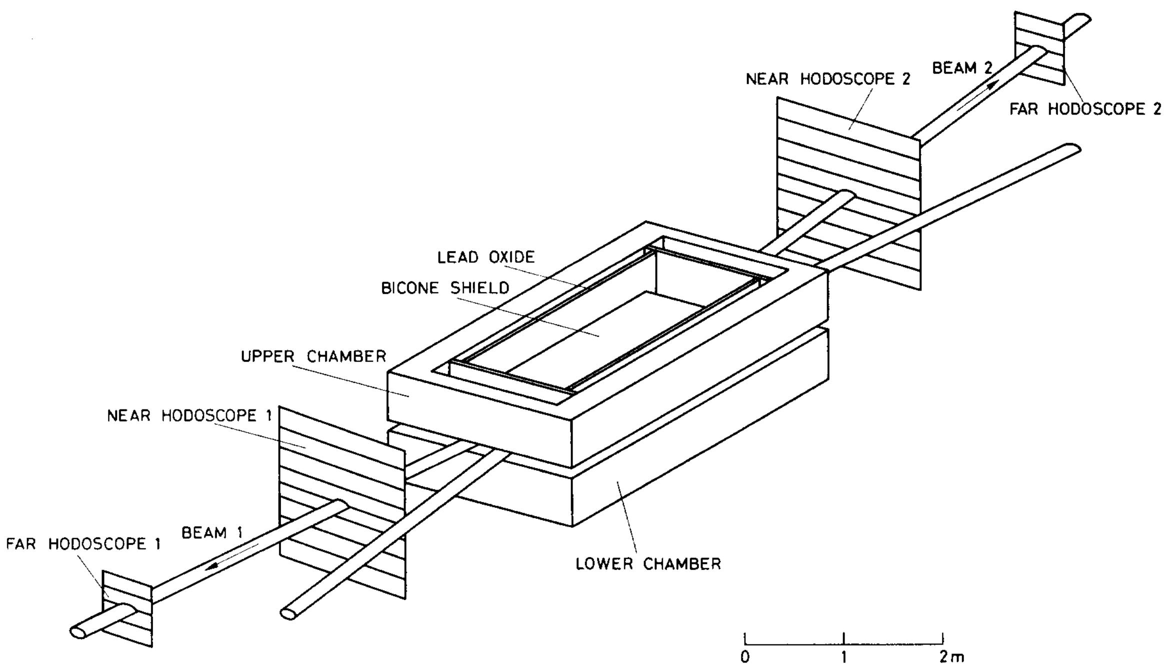

Fig. 1. Schematic layout of the apparatus. The optical system and hv generators have been omitted for clarity.

construction and performance of the apparatus, and also describe the procedure of data analysis.

2. Streamer-chamber system

2.1. Chamber design

Two identical and independent streamer chambers, one above and one below the beams, surround the ISR intersect (fig. 1). The sensitive volume of each chamber is $270 \times 125 \times 50$ cm^3. Each chamber has three parallel electrodes forming two gaps of 25 cm. The two grounded outside electrodes are joined by aluminum plates to completely enclose the streamer chambers, thus preventing them from radiating high frequencies. They are operated as transmission lines with an impedance of 25 Ω. The high-voltage pulse applied to the central electrode of each chamber is produced with a Marx generator followed by a Blumlein-line pulse shaper.

The chambers are photographed through large foil windows from above and below the intersect; therefore the central electrode and the outermost electrode in each chamber are transparent. The center electrodes and the ground electrodes towards the camera are made out of a phosphorus–bronze grid. The wire thickness of this grid is 0.13 mm, the wire spacing 1.2 mm, yielding a transparency of 80%. The inner ground electrodes and side walls of the chambers are made out of 4 mm thick aluminum plates.

The walls which define the active volume of the chambers are made of 30 mm thick PVC* plates which also provide the basic supporting frame for the whole chamber. The large foil windows of the chambers are covered by two 100 μm thick Hostafan† foils, spaced by 10 mm. These gaps are filled with helium to reduce the diffusion of impurities into the chambers.

The details of the construction around the ISR vacuum pipes and the bicone are shown in fig. 2. To obtain an almost 4π acceptance, the aluminum ground electrodes towards the intersect are cut out and replaced by epoxy resin shells, which are spray metallized with a 100 μm thick layer of zinc and

* Dynamit Nobel AG, Troisdorf, Germany.
† Kalle, AG, Wiesbaden-Biebrich, Germany.

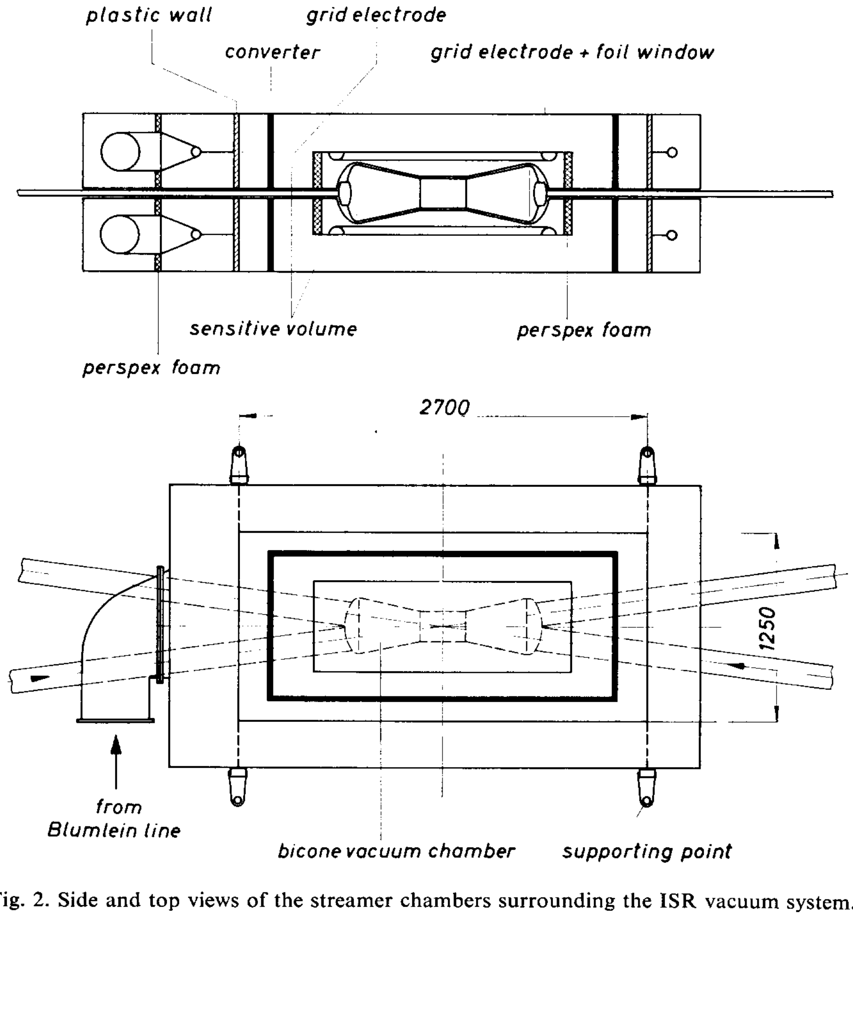

Fig. 2. Side and top views of the streamer chambers surrounding the ISR vacuum system.

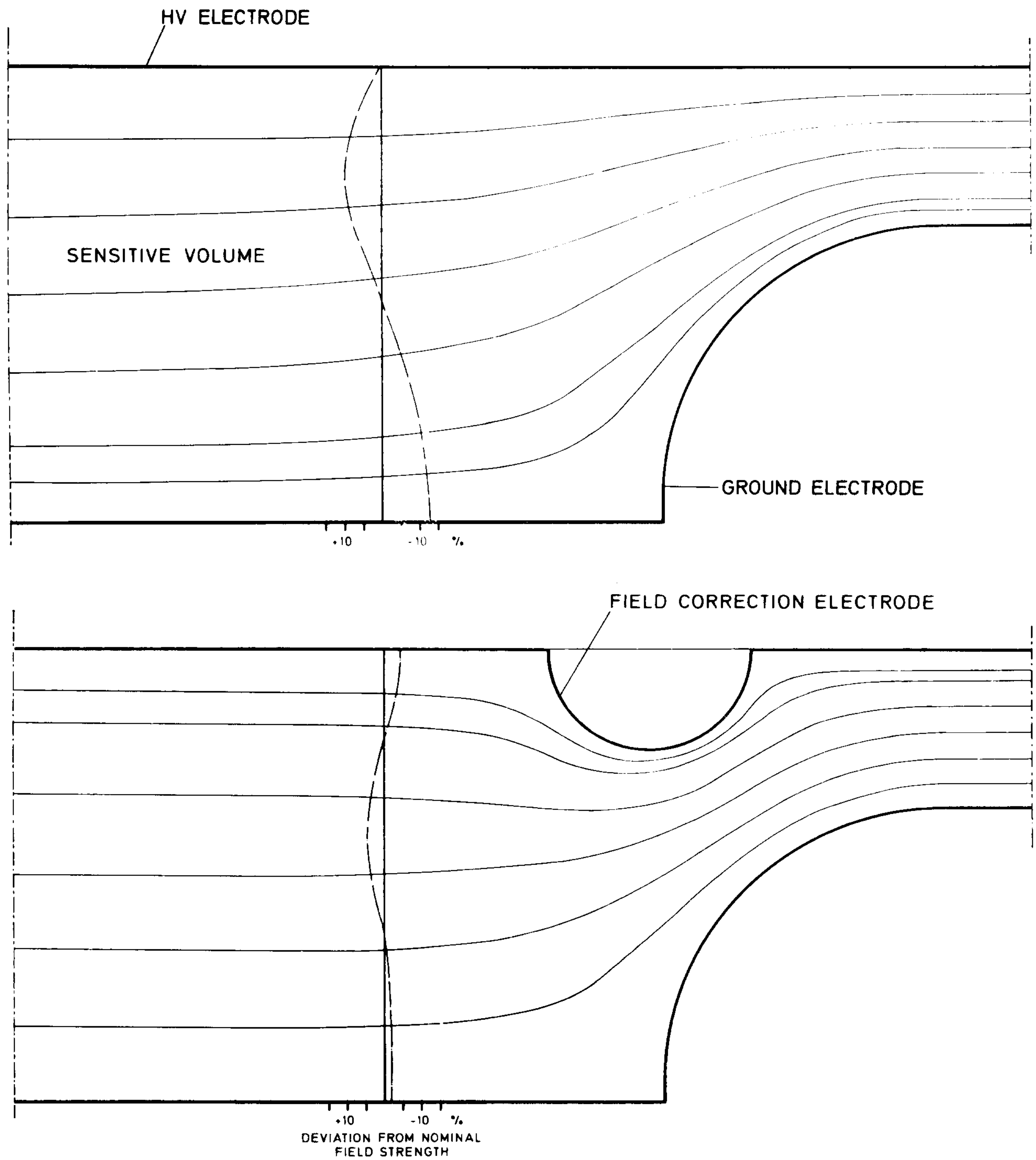

Fig. 3. Electric field in the streamer chambers near the distorted ground electrode with and without the field-correction electrodes. The deviations from the undisturbed field at the limit of the sensitive volume are indicated.

copper. They are tailored to the shape of the bicone, and strengthened with fiber glass. With this construction it is possible to surround the intersect, except for an equatorial gap of 8 cm, due to the height of the beam pipes.

The deformation of the ground electrodes strongly distorts the electric field inside the chambers. Field-correction electrodes attached to the middle electrodes localize the field distortions (fig. 3). At the bicone shields, the gap between the electrodes is only 7 cm. A box enclosing the bicone is inserted into each chamber. The boxes are made from a $70 \times 170\ \mathrm{cm}^2$ Rohacell* frame with 5 cm wall thickness. The perspex foam Rohacell is chosen because of its high mechanical stability and its large radiation length of about 10 m. The Rohacell frames are closed on top with a 1 mm thick aluminum plate, fixed to the middle electrode by means of a conducting glue. To avoid breakdowns, the boxes are flushed with a mixture of 90% N_2 and 10% Freon†.

The bicone shields also cause local changes in the impedance of the chambers. These create reflections of the high-voltage pulses and change the effective voltages in front and behind the distortions. The strength of this effect depends on the rise time of the high-voltage pulse and its length relative to the distortion. In detailed tests with a specially modified 2 m streamer chamber, it was found that the effect of the distortion is rather localized. In the final ISR streamer chambers where the sensitive region starts about 15 cm away from the field distortion, an effect on the streamer formation is hardly visible with our high-voltage pulse of 6 ns rise time and 15 ns fwhm.

To ensure an accurate positioning of the two chambers with respect to each other, four pins are attached to the outer side of each ground plate. The corresponding pins of the two chambers are aligned in such a way that a precision cylindrical sleeve can be slid from each pin to its opposite on the other chamber. All fiducial marks are measured relative to these pins and the relative position of the two fiducial systems is known to within 0.3 mm. The fiducial marks themselves are made of electroluminescent plates covered by masks with cross cut-outs.

2.2. Gamma-ray converter plates

A frame of lead-oxide plates with a thickness of 1 radiation length (2 cm) is inserted into the sensitive volume of each chamber, as shown in fig. 2. Gamma rays converting in these plates produce charged secondaries which are detected in the streamer chamber. The converter plates cover 50% of the whole solid angle. The resulting detection efficiency for γ's is 35%. The thickness of the converter plates is sufficient to stop charged pions with momenta less than 105 MeV/c.

The converter plates were made from a mixture of 83% (weight) lead-oxide (Pb_3O_4) and 17% epoxy resin. To achieve a homogeneous mixture, the two components have been rolled under high pressure. The resulting mixture was poured into moulds and hardened at a temperature of 80 °C.

Since the dielectric constant of the mixture is $\varepsilon \sim 7$–8, gaps at the junctures of the plates were carefully avoided. In such regions, the electric-field strength would be greatly increased and cause troublesome discharges. In addition to eliminating discharges from surface irregularities, we found it useful to cover the lead-oxide plates with a 2 mm thick layer of epoxy resin ($\varepsilon \sim 2.4$), thereby smoothing the change in the dielectric constant. Fiber glass is embedded into these layers to increase the mechanical strength of the plates (fig. 4).

The converter plates cause no trouble for the streamer-chamber operation, and only about 1% of charged tracks passing through the plates show small discharges on the surface.

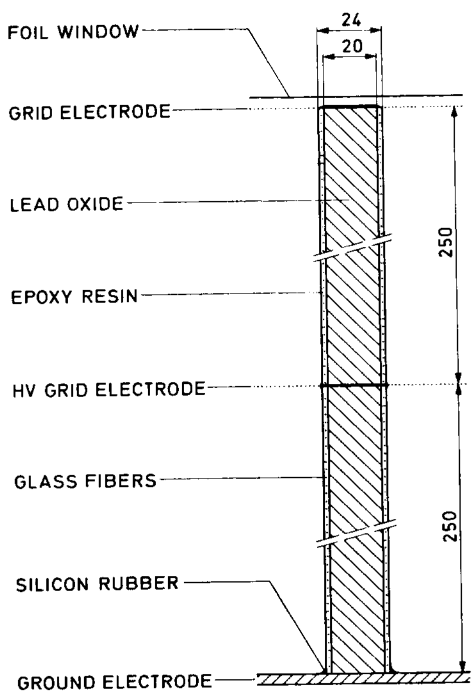

Fig. 4. Section through the lead-oxide converter plates at the junction of the plates and the hv electrode.

* Röhm, GmbH, Darmstadt, Germany.
† Kali-Chemie AG, Salzgitter, Germany.

2.3. High-voltage system

Each streamer chamber has its own high-voltage system consisting of a Marx generator and a Blumlein pulse-forming system. A 90° bend adapter provides the transition between the coaxial structure of the pulse formers and the parallel-plate geometry of the streamer chambers. The adapters are flushed with Freon to avoid corona discharges and breakdowns. Each gap of the streamer chamber is terminated with 5 resistors* in parallel, matched to the impedance of the gaps.

Each Marx generator has 17 stages which are charged to 36 kV (±18 kV). Each stage has two 10 nF foil capacitors† in parallel. The output capacity of the Marx generator is 1.2 nF. The maximum output voltage delivered to the Blumlein line is 600 kV with a repetition rate of 1 pulse/s. All spark gaps have a gap distance of 7 mm and operate under 2.3 atm N_2. They are mounted inside a single lucite cavity to allow sequential triggering via ultraviolet light to decrease the delay time. The electrodes are made from a copper–tungsten sinter. The first gap has three electrodes, one of them triggered by a 20 kV pulse, generated by a spark gap+. All elements of the Marx generators are submersed in oil. Due to the high breakdown voltage of oil, no special care needs to be taken in avoiding sharp edges and small distances, which simplifies the construction.

The output pulse of each Marx generator is shaped in an oil-filled coaxial Blumlein line[2]) with an 85 cm long charging tube. The Marx generator and the pulse former are decoupled by an inductance of about 5 μH. The capacity of the Blumlein line is 630 pF; the impedance of 25 Ω is matched to the streamer chambers. An adjustable, selftriggering spark gap in an SF_6 atmosphere discharges the Blumlein line at the desired voltage. The maximum stability of the output pulse was achieved with a flat negative electrode of 8 mm diameter with edges of about 1 mm radius, and a positive electrode which is a hemisphere of 15 mm diameter. An electrode distance of 15 mm and a SF_6 pressure of 3.5–4.0 atm gives the best working conditions, in which the spark gap fires at the beginning of the plateau of the Marx-generator pulse. The resulting pulse has a rise time and fall time of 6 ns and 8 ns, respectively, as shown in fig. 5a. The pulse length is found to be 15 ns (fwhm), which is 50% longer than expected from the length of the Blumlein line.

During data taking, it is important to have a reliable monitor for the high-voltage pulse height which determines the efficiency of the streamer chambers. Especially under bad beam conditions, the high radioactive background influences the operation of the spark gaps, causing instabilities in pulse height, and hence track brightness. For monitoring, the hv pulses are attenuated with resistor dividers and their pulse heights recorded for each event with the on-line computer. Changes of 0.1% in the pulse height are measurable. Pulse-to-pulse fluctuations are limited to 4% (fig. 5b). Typically 10% of the pictures have to be rejected for too low pulse height in one of the chambers.

2.4. Gas

The streamer chambers are operated with a mixture of 70% neon and 30% helium. A continuous flux of 3–4 l/min keeps gas impurities sufficiently low. By adding small amounts of isobutane, the necessary voltage to produce visible streamers can be reduced

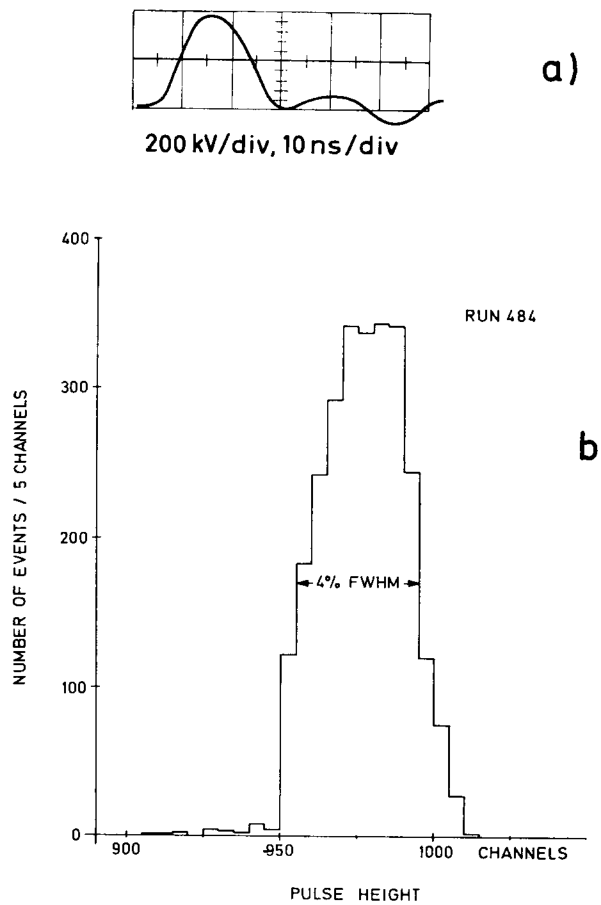

Fig. 5. a) HV pulse measured at the streamer chamber. b) Measured pulse-height distribution of the hv pulse during a data-taking run.

* Deutsche Carbone AG, Kalbach/Ts., Germany.
† Thompson–CSF, Paris, France.
+ EG&G, Boston, U.S.A.

(fig. 6). Choosing a concentration of 0.3% isobutane allows a voltage reduction of 13%, which is insensitive to small changes in the isobutane concentration and still maintains good streamer quality. To reduce the memory time of the chambers to about 2 μs, an amount of 0.1 ppm SF_6 is added (see section 2.5).

Because the lead-oxide plates prevent sufficient gas circulation between different parts of the chambers, each part is flushed individually. The chamber pressure must be controlled as the large foil windows cannot tolerate more than 1 torr pressure difference. The pressure is measured relative to the surrounding of the chambers and automatically kept constant in a range of ±0.2 torr.

The spark gaps of the Marx generators and the Blumlein pulse formers are flushed with 0.5 l/min of N_2 and SF_6, respectively. The pressure is regulated to within 0.2%.

All gases for the streamer chambers, the Marx generators, and the Blumlein-pulse forming systems are regulated by a central control system.

2.5. Memory time control

Typical ISR beams cause an interaction rate of about 10^5 interactions/s, i.e. 1 interaction every 10 μs. On the other hand, a time of 1 μs is needed to select an event with our trigger and to pulse the streamer chambers. Therefore, our memory time was chosen to be in the region of 1–2 μs.

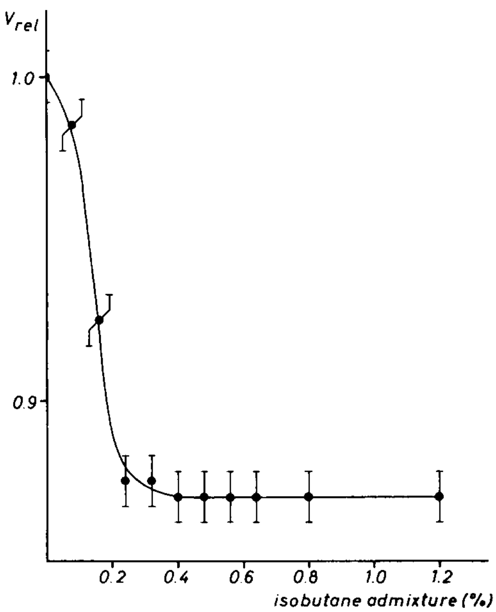

Fig. 6. Voltage needed to obtain streamers of a given length as a function of the isobutane admixture.

The memory time is determined by the lifetime of free electrons and conventionally measured by the exponential time constant of the streamer density. For noble gases, the memory time is of the order of a few hundred μs. It can be shortened by adding an electronegative gas which attaches free electrons. An amount of 0.1 ppm SF_6 is needed to reduce the memory time to 1–2 μs. Since the SF_6 molecules are cracked by gas discharges and radiation, one has to control its concentration.

The concentration is monitored with small ionization chambers[3]), which are connected to the gas outlets of the streamer chambers. In each ionization chamber, free electrons are produced by an α-source and drift in an electric field. The electrons not captured by the SF_6 are collected at the anode; the resulting current is a measure of the memory time. This current is compared with a reference value and, if necessary, an injection valve adds an amount of 10 mm^3 (~0.007 ppm) SF_6 to the neon-helium flux of the streamer chambers. A 30 l gas tank after the injection valve is used as a mixing volume. At normal running conditions, the memory time in the chambers is about 2 μs, corresponding to curve c in fig. 7.

3. Optics

The optical system was kept as simple as possible, since only straight tracks are to be measured, and stereoscopic photography with moderate accuracy and resolution is sufficient. Two stereo views per chamber recorded on 50 mm (later 35 mm) film were found to be adequate for this purpose. For convenience in scanning and measuring, the two views of each chamber should be close together and are photographed through a single lens. For reasons of isotropy and efficiency of

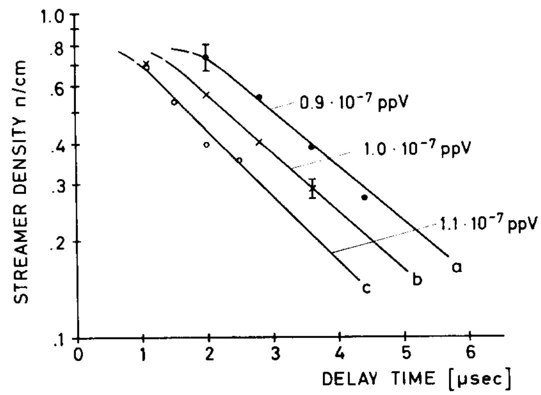

Fig. 7. Measured streamer density for different SF_6 concentrations as a function of the delay time between the interaction and the hv voltage pulse.

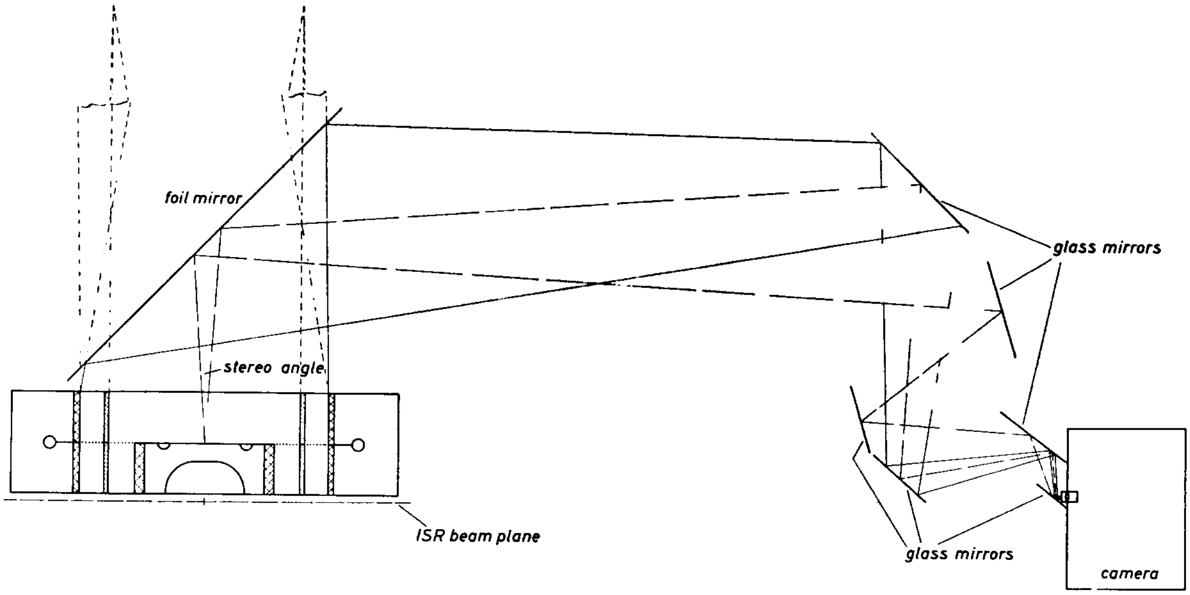

Fig. 8. Schematic layout of the optical system for the upper streamer chamber. The system for the lower chamber is identical.

the streamer chambers, it was necessary to use image intensifiers.

In the following sub-sections, we discuss the elements of the optical system: mirrors, lenses, image intensifiers, the camera, and finally, the method of calibration.

3.1. Mirror system

The chambers must be viewed vertically through their transparent mylar windows. To bring the images to a single camera, and to achieve a stereo view, a series of mirrors is used, as shown in fig. 8 for the upper chamber; the system for the lower chamber is symmetric. The camera is located at beam height on the perpendicular to the long dimension of the streamer chambers. The optical path length was chosen to be 7 m to obtain a 4 cm image on the original 50 mm film, using a lens of 100 mm focal length. The two views of each chamber are photographed through the same lens. The rays of each view which strike the chambers at 90° were chosen to intersect the mid-point of the long lead-oxide converter plates, minimizing the shadows caused by the plates. As the plates are 1 m apart, the stereo angle is then 8°.

With this arrangement, one achieves an optimal stereo effect in the densely populated forward regions. The endpoint of a track is always visible in both views to allow track matching by means of corresponding points. For production angles of 90° where the tracks are in the plane of the optical axes, depth reconstruction depends upon the use of corresponding points.

The mirrors directly after the chambers are made of aluminized Mylar* foil, stretched under heat over a sharp-edged frame accurately milled to ensure a flat surface. The frame is kept rigid by a lightweight honeycomb† supporting structure. The reflectivity was measured to be 90%, and the surface quality is such that less than 2% of the light is scattered by more than 0.3 mrad. Thus, from a narrow strip (~2 cm) along the edges, these mirrors induce neither appreciable light diffusion nor distortions. The other mirrors are made of glass plates with a magnal+ layer and protected by a thin quartz coating. The reflectivity of the complete mirror system was measured to be 60%.

3.2. Lenses and image intensifiers

For simplicity, we first tried to photograph the tracks directly on 50 mm film Kodak SO 265**. The most suitable lens which used the full size of the film was a Deltamar†† lens ($f/d = 1.4, f = 100$ mm). In our system, this lens gave a demagnification of 70 and a resolution at the maximum aperture of 25 line pairs/mm on film over the entire 60 mm image diameter. With light losses due to the mirror system (~40%), the grid electrodes of the chambers (~35%), and the vignetting of the lens (~35% at the image edges), a

* Guest Industrials AG, Zug, Schweiz.
† Ciba-Geigy UK Limited, Duxford, Cambridge, England.
\+ Hereaus, Hanau, Germany.
** Kodak, Rochester, U.S.A.
†† De Oude Delft, Delft, Netherlands.

streamer length of 20–30 mm was needed to provide enough light to photograph horizontal tracks in the forward directions.

With this streamer length, the brightness of tracks strongly depends on their angle to the electric field. Steep tracks which are much brighter than horizontal tracks often enter the spark mode, overexposing large areas of the film. Furthermore, conversion electrons emerging from the bottom plates of the chambers caused flares which obscured large regions. To avoid these effects and ensure a good detection efficiency in all parts of the chambers, the streamer length had to be limited to 15 mm. But this streamer length was not sufficient for photography of forward tracks which are most affected by the optical system.

To overcome these difficulties we used image intensifiers.

The necessity for compactness and simplicity led to the choice of an electrostatic single-stage image intensifier (RCA 8505/V1*). This tube requires only a dc voltage of 15 kV. It has a light amplification of about 85 at 600 nm and an excellent long-time stability. The tube requires no adjustment and is therefore well suited to remote operation inside the ISR tunnel.

The Zeiss Planar objective† ($f/d = 1.4$, $f = 50$ mm) was chosen as being the best match to the image intensifier which has a useful diameter of 30 mm. With the 50 mm lens the demagnification is 140 and the two stereo views lie in a 20 mm square. Although the new lens has the same f/d ratio as the old, the light intensity on the film is reduced by a factor of 4 as the size of a "point" on film does not decrease appreciably for demagnifications above 50. The actual light amplification achieved by the use of image intensifiers is a factor 10–20. Fig. 9 shows the measured resolution of the image intensifier itself, the lens together with the image intensifier, and finally, the resolution obtained on the film.

The resolution on film is the same as in the case of direct photography, but due to the higher demagnification (140) the resolution in the streamer chamber is now two times worse. The minimal streamer size on film is 50 μm, corresponding to about 7 mm in real space. Tracks with angles less than 30° relative to the electrical field appear much thicker (200 μm).

Since steep tracks which may overexpose the film only appear in the central regions of the streamer chambers, we covered these regions with light-absorbing foils. These foils have a transparency of about 50% and shade an area of 140×64 cm^2 of the foil windows.

A further improvement was achieved by using a new film from Kodak (SO 121); this film has an antihalation layer between the emulsion and the Estar base, diminishing light reflection at the backing. In com-

* RCA, Harrison, U.S.A.
† Carl Zeiss, Oberkochen, Germany.

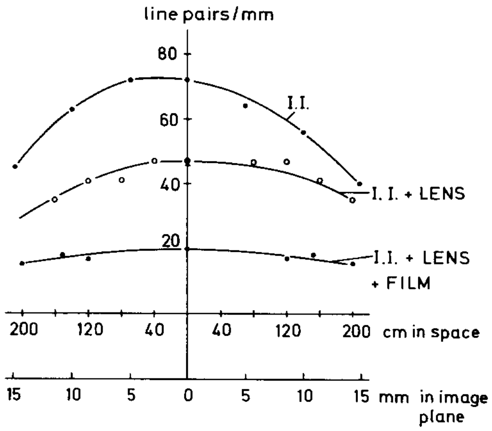

Fig. 9. Measured resolution as a function of the distance from the optical axis for the image intensifier (I.I.) and lens (Planar 50 mm, $f/d = 1.4$) and the entire system consisting of image intensifier, lens, and film (Kodak SO 121).

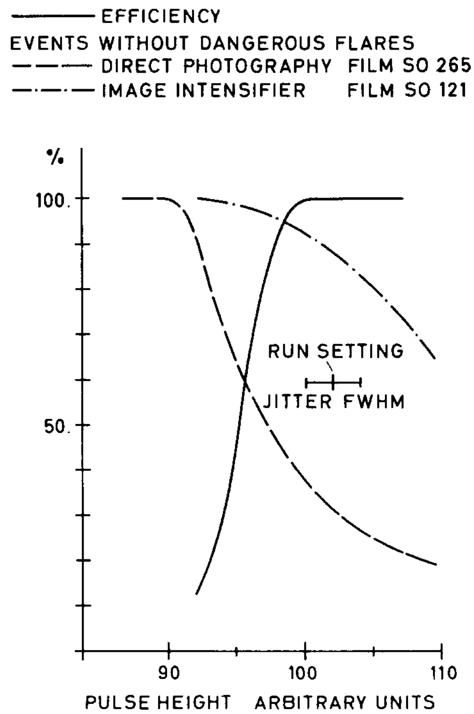

Fig. 10. Measured efficiency of the streamer chambers (solid line) and number of pictures without dangerous flares (dashed line) as a function of the pulse height, using direct photography with film SO 265, and using image intensifiers with film SO 121.

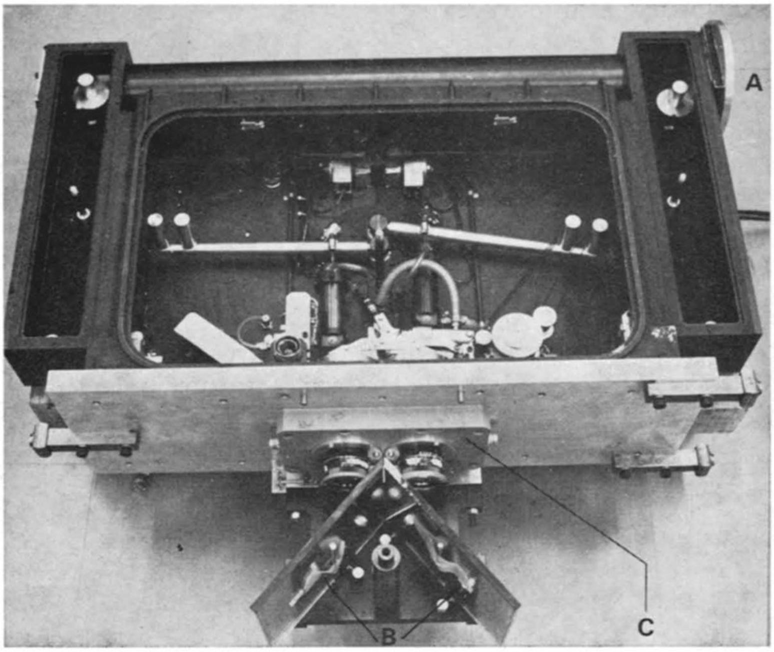

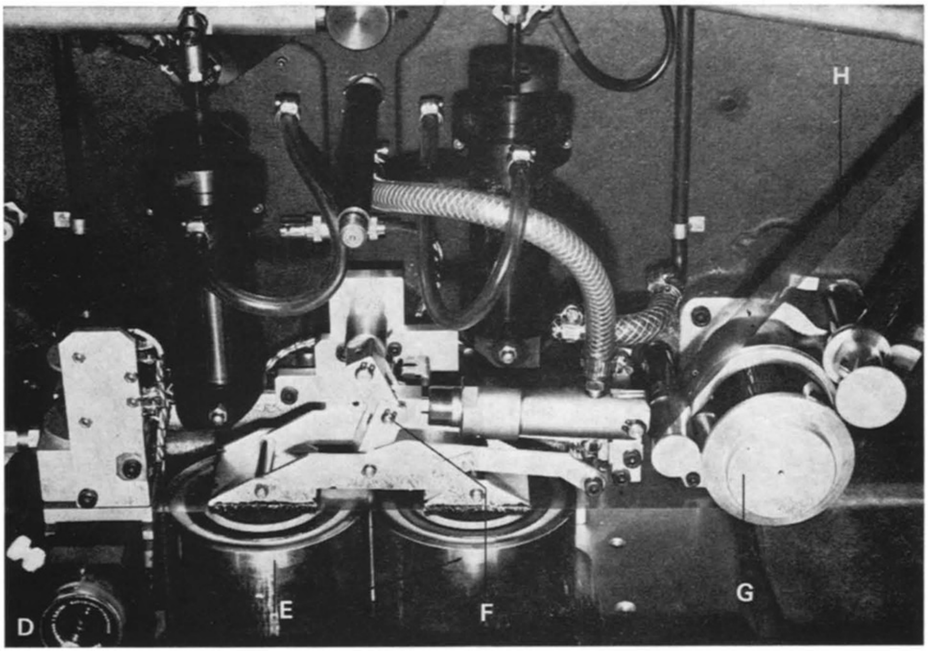

Fig. 11. Top: photograph of the camera and the last 45° mirror of the optical system of each chamber. A: towards magazines, B: 45° mirrors, C: image-intensifier mounting plate. Bottom: photograph of the camera showing, in detail, the two image intensifiers and the film-pressing mechanism. D: lens of data-box optics, E: image intensifier, F: film-pressing mechanism, G: vacuum capstan, H: film.

parison to the SO 265, the new film reduced the number of overexposures by 30%.

The effect of these improvements is demonstrated in fig. 10, which shows the detection efficiency for tracks in the forward directions together with the fraction of pictures without dangerous flares as a function of the high-voltage pulse. Tolerating a pulse jitter of 4% led to more than 80% of the pictures with almost no flares and 100% detection efficiency at the same time. This was impossible to achieve in the case of direct photography using film SO 265.

3.3. Camera, data box, and film transport

A single camera is used to photograph the four views of the two streamer chambers, as well as digital displays on a data box.

The camera optics consist of 2 symmetric configurations of a 45° mirror, a Zeiss Planar lens, a shutter, and an RCA 8505/V1 image intensifier all mounted on a single support (fig. 11 top). For insulation, the image intensifiers are encased in silicon rubber and shielded against stray magnetic fields by μ-metal cylinders. It is not necessary to shield the image intensifiers against ionizing radiation. The shutters are always open in normal operation, and only closed during the light-flash excitation of the calibration grid (section 3.4).

The film is pressed directly against the fibre optic output window of the image intensifiers for exposure and released during transport (fig. 11 bottom).

In addition to the views of the chambers, the camera records the run and event numbers and the Blumlein high-voltage pulse heights which are displayed on a data box. The optics for this consist of a third lens (1:5.6/60 mm) mounted on the side of the camera (fig. 11a, b) followed by a small 45° mirror inside the camera to reflect the image onto the film. An event occupies 23 cm of film in separate images of the two chambers and the data box. To conserve film, consecutive events are interleaved allowing 6 events per meter. Although the film is unperforated, accurate positioning of the film to avoid superimposed images was made possible by the use of a vacuum capstan wheel.

The camera is operated remotely inside the ISR tunnel without access during runs for up to 50 hours. To allow the film to be changed at more frequent intervals, and to avoid its being exposed to radiation for long periods, the film magazines are located outside the tunnel. The film is transported to and from the camera inside an 11 meter light-tight tube, guided over a series of rollers.

3.4. Calibration grid

Distortions of the images are caused by the image intensifiers, the wide-angle optics, and possible instabilities of the mirror system. For the necessary distortion corrections, a large number of accurately positioned reference points have to be established. Hence, each chamber was permanently equipped with a large calibration grid (260×120 cm^2) made of a 16×10 net of phosphor-coated nylon wires. The wires are stretched between precisely notched invar gauge rods, supported by an aluminum frame (300×150 cm^2, 11 kg) mounted outside the Mylar window of each chamber. The crossing points of the wires supply 160 reference points which are known with an accuracy of 0.1mm.

Calibration pictures of the grid are regularly taken. For this, two photo flash lamps are fired which excite the phosphor. The decay time of the luminescence is 10 s and its light is sufficient to expose the film. When the lamps are flashed, the two shutters in front of the lenses are closed to protect the image intensifiers. The method of flash-lamp photography employed here is rather the inverse of the usual in that the shutters of the lenses are normally open and are closed only when the lamps are fired.

4. The trigger

The chambers are triggered on beam–beam interactions by scintillator hodoscopes on both downstream arms, or by interactions including a photon in a lead-glass Cherenkov counter located at 90° to the beam directions.

4.1. Scintillation counters

The hodoscopes in each arm (fig. 1) consist of two separate planes of counters at 3 m (near hodoscope) and 5 m (far hodoscope) distance from the intersect. The near hodoscopes are made of 8 horizontal counters, 150 cm in length; the outer six are 22 cm wide, the inner two are 10 cm wide. They cover production angles from about 20 mrad to 250 mrad. The two far hodoscopes, 50×60 cm^2 in size, detect particles produced at small angles ($\vartheta_{\min} = 6$ mrad). All counter planes are doubled. A coincidence of adjacent counters in two layers is used to suppress background from induced radio-activity. The 150 cm long counters are viewed by photomultipliers from both ends. The OR's of near and far hodoscopes in each arm define the arm 1 (arm 2) signals. The coincidence of arm 1 and arm 2 is used as a trigger. At a center-of-mass energy of $\sqrt{s} = 53$ GeV, about 95% of all inelastic events trigger the scintillation counters, partially due to γ-rays converting in the lead-oxide plates of the streamer chambers.

Particles coming from upstream are vetoed by a coincidence between an upstream anticounter and one of the downstream counters. The incoming beam pipes were surrounded by shielding material. Beam–beam interactions are separated from background by measuring the time-of-flight between arm 1 and arm 2 signals. The fwhm of the beam–beam signal is 7 ns. The trigger window of 15 ns rejects all but 1 % of the background from stray particles. In normal running conditions, the rate of accidental triggers at luminosities around 10^{30} cm^{-2} s^{-1} never exceed 0.1 %.

The luminosity is monitored using a four-fold coincidence of the inner near and the far counters of both arms. Background and accidental rates in the arm–arm coincidence of these telescopes are suppressed to a level of 10^{-4}.

Two small-acceptance telescopes define a trigger used to monitor the efficiency of the streamer chambers in a well-defined region of each chamber.

4.2. Lead-glass Cherenkov counter

A lead glass Cherenkov counter[4]) provides a trigger on high-transverse-momentum γ-rays. It consists of 61 hexagonal blocks of 13.6 cm diameter (inscribed circle) and 33 cm length (15 radiation lengths), which are arranged in the form of a large hexagon with a total area of about 1 m^2. The counter is located at 90° from the beam direction at a distance of 1.9 m and subtends a solid angle of 0.3 sr in the center-of-mass system. It is shielded against background from both rings by 1.8 m of iron. This shield also protects the counter from radiation during beam stacking.

An anodeand a dynode signal is derived from each photomultiplier. The dynode signals are added in linear mixers. A trigger is given when the dynode sum exceeds an adjustable threshold. Since the pulses from the photomultipliers have long rise times (20 ns), a second discriminator operates at low threshold to define the timing independent of pulse height. The trigger requires a coincidence within 50 ns with a beam–beam signal from the scintillation counters. Under good beam conditions and at 2.5 GeV threshold, the coincidence rate is half of the signal rate in the Cherenkov counter. Accidental coincidences, typically less than 1 %, of Cherenkov, arm 1 and arm 2 counters are continuously recorded.

The anode signals are measured with 8-bit ADCs and recorded with the on-line computer. These pulse heights were calibrated in an electron beam and are regularly monitored by a system of light diodes. In addition a NaI (^{241}Am) light source, equivalent to 2.4 GeV energy, is used to perform calibrations in larger time intervals.

4.3. Streamer-chamber trigger

The time difference between an interaction and the arrival of the two high-voltage pulses at the streamer chambers is 1 μs, 200 μs due to delay in the fast electronics, 500 ns due to cable delays, and 300 ns due to delays in the hv system. A second beam–beam interaction which occurs within this time interval will also be made visible by the same hv pulse. During the first 800 ns after a trigger, such an interaction is detected by the scintillation counters and so can be tagged and excluded from scanning and measuring. The remaining 20 % cannot be tagged because the Marx generator pulse is 200 ns earlier than the fast hv pulse and induces noise on the signal cables. Some of the untagged double events can be identified in the pictures by a sufficient separation of their vertices since the interaction region extends over 40 cm.

The trigger is inhibited for 5 μs after each beam–beam coincidence to ensure that there is no memory of this event at the time of a subsequent trigger.

5. Measurement and performance

5.1. Distortion corrections and optics calibration

The spatial reconstruction of tracks is done in an idealized optical system with tilted optical axes and pinhole camera optics. The distortions introduced by the lens–image-intensifier system (up to 250 μm at the edge of the 20 × 20 mm^2 picture area) are computed and corrected with the help of the calibration grid and the fiducial system on the chambers (fig. 12).

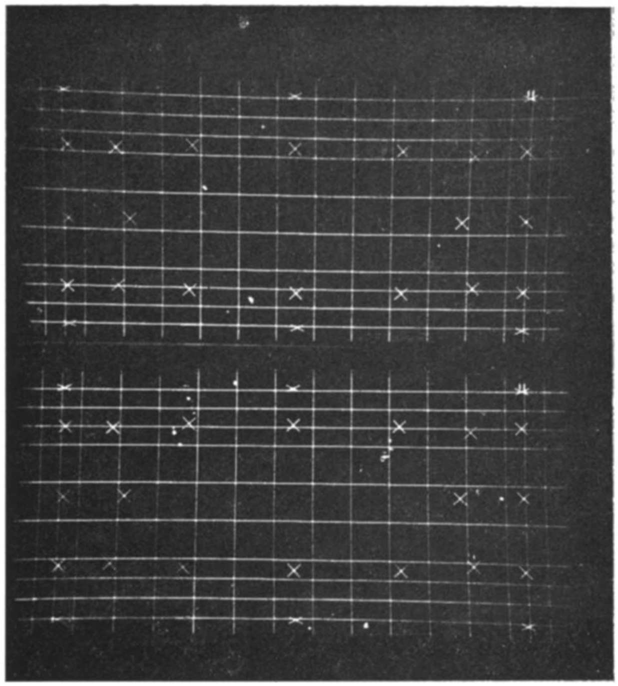

Fig. 12. Photograph of the two views of a calibration grid with fiducial marks.

Using the measured nodal-point positions as a first approximation, the distortions at the grid points are computed and fitted to a distortion polynomial with 14 coefficients. The remaining distortions, typically 20 μm on the film, are removed by a linear interpolation between the nearest four grid points. We estimate an uncertainty of ~ 15 μm for the overall correction, due to the measuring errors on the grid pictures.

Measurements of the chamber fiducials are then used to fit the exact nodal-point positions. An iteration of this two-step fit procedure was found unnecessary.

In order to test the effect of variations of the hv on the image intensifiers, grid pictures were taken at several voltages. Reducing the hv from 15 kV (our normal setting) to 12 kV, the magnification variation of the intensifier caused a change of only 40 μm over the full picture diagonal (24 mm). Since we used a stabilized hv supply, the effects of voltage variations are negligible.

5.2. Scan and measurement

The pictures (fig. 13) are scanned and measured on image-plane digitizing projectors. All tracks pointing to the interaction region within 15 cm in space are measured in each view with 3 points; the endpoint is always a corresponding one. About 20 min are required to scan and measure a typical event of 15 tracks. The setting error of the measurement is 12 μm on film (36 μm for steep tracks). Track losses due to flares and overlapping tracks (more serious for steep tracks) are less than 1%.

The tracks are reconstructed as straight lines in space, using the two stereo views. Typical uncertainties of the track extrapolation to the interaction region are 0.6 cm (8 cm) in the horizontal (vertical) projection. The interaction point is found by an iterative least-squares fit to all the measured tracks. At each iteration, the worst tracks are rejected until all remaining tracks fit to the vertex within 2 standard deviations. The errors on the final vertex position are about 0.3 cm (4 cm) in the horizontal plane (vertical direction). Finally, the production angles of all tracks are refitted using the horizontal vertex coordinate, and the known beam height as additional constraints. Fig. 14 gives the dis-

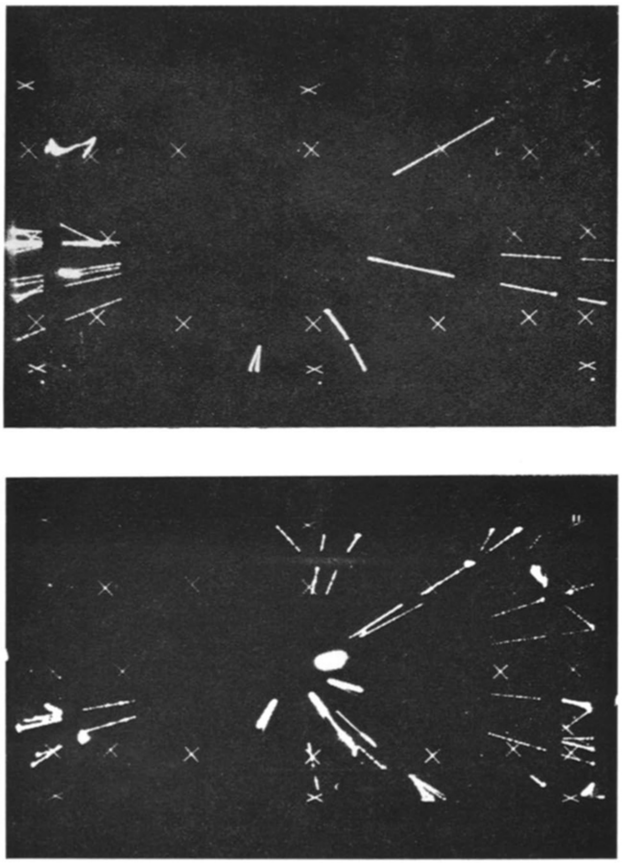

Fig. 13. Photographs of two typical events.

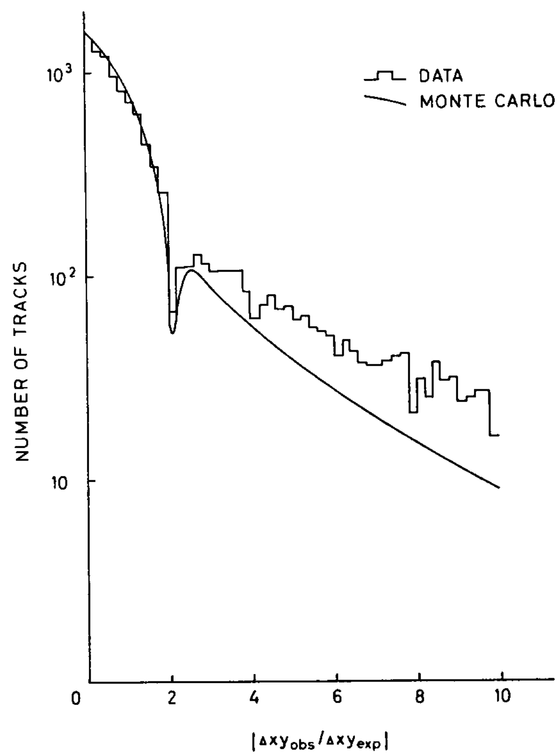

Fig. 14. Observed deviation in horizontal plane of tracks from the fitted vertex position divided by the expected deviations due to the reconstruction accuracy for data (histogram) and for a Monte Carlo study (smooth curve).

tances to the vertex, divided by the errors of the tracks in the horizontal plane. Tracks which deviate from the vertex by more than 3 standard deviations are rejected.

The track reconstruction errors are well reproduced by a Monte Carlo study (dashed curve in fig. 14) which includes the effect of the setting error as well as multiple Coulomb scattering and secondary interaction of pions and photons in the walls of the streamer chambers and the vacuum chamber. The study also estimates about 10% of reconstructed tracks to be electrons from converted photons, primarily at small angles to the beams (fig. 15). The acceptance for charged tracks as a function of the pseudo rapidity η is shown in fig. 15.

The errors in the azimuthal angle φ and in the pseudo rapidity due to reconstruction errors are shown in fig. 16.

6. Summary

The streamer-chamber system described here was a successful solution to the need for a large-solid-angle multiple-particle detector operable at the CERN ISR. Several novel features were essential to obtain optimal performance under the ISR conditions and to meet the experimental requirements:

- The ground electrodes of the chambers were deformed to accommodate the complex structure of the ISR vacuum chamber with minimum loss of solid angle.
- Lead-oxide converter plates inside the active volume of the chambers detected 35% of all photons produced.
- Image intensifiers were used allowing the entire chamber to be photographed through a single lens with excellent stability.
- The chamber memory time was maintained at 2 μs to allow data collection at interaction rates as high as 200 kHz.

The simplicity of the apparatus permitted its installation within 7 months of the beginning of construction. In 10 months of running, 330 000 pictures were taken. A significant sample of the data has been analyzed and the first results are published[5]).

We thank Profs. H. Faissner and N. Schmitz for encouragement and support. Many other people have helped to make this experiment possible. We are indebted to Messrs. H. Geissmann, E. Giesche and their colleagues for their skillful and quick work in building the streamer chambers, and to Messrs. D. Bernier and W. Tribanek for their design work. For the camera as well as the complicated mirror system we are grateful to Dr G. Muratori and his colleagues Messrs. R. Baum, A. Domeniconi, G. Gendre and K. Harrison. For designing and building parts of the electronics we thank Mr H. Utzat and his colleagues and Mr G. Hilgers. The success of the experiment has also depended upon the help during the installation at the ISR by Messrs. B. Couchman and J. Renaud and the technical assistance of Messrs. V. Beck, J. M. Chapuis, E.

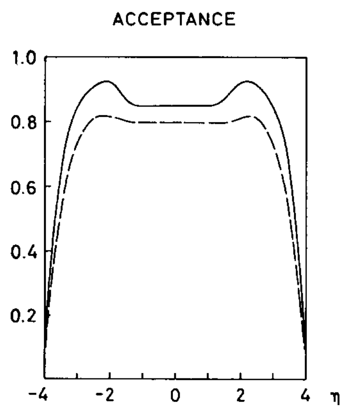

Fig. 15. Solid curve: Acceptance of the streamer-chamber system for charged particles as a function of the pseudo rapidity η. Dashed curve: Acceptance for charged hadrons after removing the electron contamination due to photon conversion in the vacuum chambers and the streamer-chamber walls.

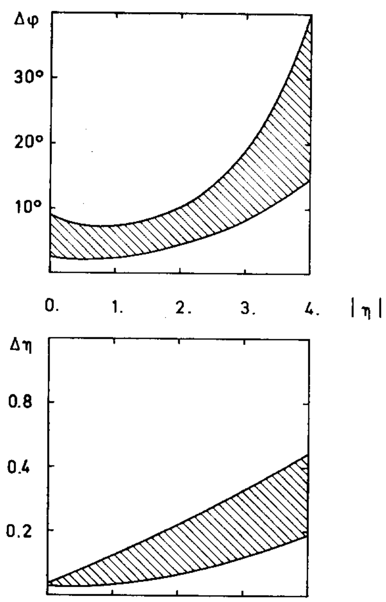

Fig. 16. a) Error in the azimuthal angle φ due to the reconstruction accuracy as a function of pseudo rapidity η. b) Error in the pseudo rapidity η due to the reconstruction accuracy as a function of η.

Hermens, S. Lipp, J. Ritzer and F. Wondrasch. We also thank the ISR staff for providing excellent operating conditions. The careful development of our film by Mr J. C. Catin and his colleagues is gratefully acknowledged. Mrs P. Rimmer and Mr M. Sendall have been very helpful in setting up the on-line computer-programs. The lengthy task of scanning and measuring has been performed with perseverance and care by the scanning teams in the four laboratories.

Partial financial support was given by the Bundesministerium für Forschung und Technologie.

References

1) CERN Internal Report ISR-EN-71-25, unpublished.

2) V. Eckardt and A. Ladage, Proc. Symp. on *Nuclear electronics* (Versailles, III, 10-1 1968).

3) V. Eckardt and H. J. Gebauer, DESY 72/2 (February 1972).

4) M. Holder, E. Radermacher, A. Staude, P. Darriulat, J. Deutsch, J. Pilcher, C. Rubbia, K. Tittel, C. Grosso-Pilcher, M. Sciré and A. Villari, Nucl. Instr. and Meth. **108** (1973) 541.

5) K. Eggert, H. Frenzel, W. Thomé, B. Betev, P. Darriulat, P. Dittmann, M. Holder, K. T. McDonald, T. Modis, H. G. Pugh, K. Tittel, I. Derado, V. Eckardt, H. J. Gebauer, R. Meinke, O. R. Sander and P. Seyboth, Nucl. Phys. **B86** (1975) 201.